RESEARCH ARTICLE | DECEMBER 18 2024

Photodissociation of the CH_2Cl radical: A high-level *ab initio* study

F. Charfeddine ; O. Yazidi ; A. Zanchet ; L. Bañares ; A. García-Vela

J. Chem. Phys. 161, 234304 (2024)
https://doi.org/10.1063/5.0243800

The Journal of Chemical Physics ARTICLE pubs.aip.org/aip/jcp

Photodissociation of the CH_2Cl radical: A high-level *ab initio* study

Cite as: J. Chem. Phys. 161, 234304 (2024); doi: 10.1063/5.0243800
Submitted: 14 October 2024 • Accepted: 3 December 2024 •
Published Online: 18 December 2024

F. Charfeddine,[1,2] O. Yazidi,[1] A. Zanchet,[2] L. Bañares,[3,4] and A. García-Vela[2,a)]

AFFILIATIONS

[1] Laboratoire de Spectroscopie Atomique, Moléculaire et Applications-LSAMA LR01ES09, Faculté des Sciences de Tunis, Université de Tunis El Manar, 2092 Tunis, Tunisia
[2] Instituto de Física Fundamental, Consejo Superior de Investigaciones Científicas, Serrano 123, 28006 Madrid, Spain
[3] Departamento de Química Física, Facultad de Ciencias Químicas, Universidad Complutense de Madrid (Unidad Asociada I+D+i CSIC), 28040 Madrid, Spain
[4] Instituto Madrileño de Estudios Avanzados en Nanociencia (IMDEA-Nanoscience), 28049 Madrid, Spain

[a)] **Author to whom correspondence should be addressed:** garciavela@iff.csic.es

ABSTRACT

Photodissociation of the CH_2Cl radical is investigated by using high-level multireference configuration interaction *ab initio* methods, including the spin–orbit coupling. All possible fragmentation pathways, namely, $CH_2Cl + h\nu \rightarrow CH_2 + Cl$, HCCl + H, and CCl + H_2, have been analyzed. The potential-energy curves of the ground and several excited electronic states along the corresponding dissociating bond distance of each pathway have been calculated. Inclusion of the spin–orbit couplings is found to be crucial because it strongly determines the shape of the curves of the different excited states and, therefore, their photodissociation dynamics behavior. Analysis of the potential curves indicates that the pathways producing CH_2 + Cl and HCCl + H can occur through a fast direct dissociation mechanism, while the pathway leading to CCl + H_2 involves much slower dissociation mechanisms such as internal conversion between electronic states, predissociation, or tunneling through exit barriers. The main implications are that the two faster channels are predicted to be dominant, while the slower pathway is expected to be very unlikely and rather irrelevant. Appreciable actinic fluxes of solar irradiation are available at stratospheric altitudes where ozone is abundant, in the wavelength range where absorption of the first low-lying excited states of CH_2Cl has been observed experimentally. Our results show that in this excitation energy range, the above-mentioned two dominant dissociation pathways are open and then could contribute to stratospheric ozone depletion.

I. INTRODUCTION

The photochemistry of radicals and reactive intermediates is important in atmospheric chemistry.[1] In particular, halocarbon radicals play an active role in atmospheric reactions[2,3] and specifically in gas phase reactions with ozone, producing carbon monoxide. In addition, photodecomposition of halocarbon radicals is a well-known source of halogen atoms in the atmosphere. Atomic halogens (X = Cl, Br, I) are among the main causes of depletion of ozone ($X + O_3 \rightarrow XO + O_2$) in the stratosphere and troposphere[4,5] and have an indirect cooling effect on climate.[6] Thus, investigating the photodissociation of these halocarbon radicals in the spectral regions where the solar actinic flux is high provides valuable information about their atmospheric behavior and particularly in relation to ozone depletion. Here, we explore the photodissociation dynamics of the CH_2Cl radical and its relevance for the atmospheric chemistry.

The CH_2Cl radical can be generated through different reactions, some of them starting from either CH_3Cl or CH_2ClX (X = Cl, Br, I),[7–16]

$$CH_3Cl + R \rightarrow CH_2Cl + HR, (R = OH, F, Cl), \quad (1)$$

$$CH_2Cl_2 + R \rightarrow CH_2Cl + ClR, (R = F, Cl), \quad (2)$$

$$CH_2ClR + h\nu \rightarrow CH_2Cl + R \ (R = Cl, Br, I). \quad (3)$$

Similarly, reactions with different atmospheric reagents such as O_2, OH, HBr, Cl_2, O, and Cl contribute to the destruction of the CH_2Cl

radical.[9–11,14,15,17,18] Photodissociation in the atmosphere constitutes another important CH_2Cl decomposition alternative.[12,13]

Several theoretical studies on the electronic structure of the CH_2Cl radical have been published. Applying an *ab initio* second-order Møller–Plesset (MP2) level of theory, the transition states of the $CH_2Cl + Cl_2$ reaction were calculated in order to rationalize experiments on the kinetics of this reaction in the ground state.[11] A few years later, Li and Francisco reported the first complete active space self-consistent-field (CASSCF) and multireference configuration interaction (MRCI) studies on the ground and several first excited states of CH_2Cl, reporting vertical excitation energies (VEEs).[19] Later the same year, Levchenko and Krylov[20] reported VEEs calculated at equation-of-motion coupled-cluster singles and doubles (EOM-CCSD) and configuration interaction singles (CIS) levels of theory, as well as at time-dependent density functional theory (TD-DFT) level. In this latter study, the number of excited states investigated was increased. These two works[19,20] concluded that the equilibrium geometry of CH_2Cl was planar. Coupled-cluster calculations also including triple excitations [CCSD(T)] were also carried out later.[21] In a further work,[13] the potential-energy curves (PECs) of the ground and the two lowest excited states of symmetry $^2A_1$ of CH_2Cl and the interactions between them, were calculated using the CCSD and the EOM-CCSD methods and were used to understand photodissociation experiments carried out by Reisler and co – workers.[12] More recently, the stationary points of the reactions $CH_2Cl + O_2$,[14] and $CH_2Cl + NO_2$,[22] were investigated using density functional theory (DFT).

The CH_2Cl radical has also been the subject of several experimental studies. The first CH_2Cl ultraviolet absorption spectrum between 197.5 and 230 nm was reported more than forty years ago.[9] Far-infrared laser magnetic resonance spectra of this radical in the $\tilde{X}\ ^2B_1$ ground electronic state were also measured.[23] The kinetics and rate constants of the reactions of CH_2Cl with different species such as CH_2Cl,[9] HBr,[17] O,[10,15] Cl_2,[11,18] and O_2,[14] have been experimentally explored. Experiments of CH_2Cl photodissociation into $CH_2 + Cl$ at different excitation wavelengths have been carried out.[12,13,24]

The main goal of the work reported here is to investigate the photodissociation of the CH_2Cl radical through all the possible fragmentation pathways and to analyze its possible role in atmospheric chemistry. Photolysis of CH_2Cl can take place through the dissociation pathways,

$$CH_2Cl + h\nu \rightarrow CH_2 + Cl, \tag{4}$$

$$CH_2Cl + h\nu \rightarrow HCCl + H, \tag{5}$$

$$CH_2Cl + h\nu \rightarrow CCl + H_2. \tag{6}$$

Among the above-mentioned fragmentation pathways, pathway (4) is the atmospherically most relevant one because it directly produces atomic chlorine that may contribute to ozone depletion. This is the reason why this pathway has been that most extensively studied, both experimentally and theoretically.[12,13,19,24] Pathways (5) and (6) are also interesting because they produce other chlorocarbon radical species that can be intermediates in several atmospheric chemical processes and cycles. Further photodissociation of these intermediate radicals could be additional sources of Cl atoms.

The above-mentioned pathways were investigated by applying highly correlated *ab initio* methods, by calculating the PECs of the ground and several excited electronic states along the corresponding dissociation coordinates. In particular, the PECs of pathways (4)–(6) were computed at MRCI level of theory including the spin–orbit coupling. Thus, the present work applies a higher level of theory than the previous *ab initio* studies[13,19–21] of the CH_2Cl photodissociation, which did not include spin–orbit effects. This work also extends the investigation of the CH_2Cl photolysis to pathways (5) and (6) which, to the best of our knowledge, are largely unexplored so far. Actually, these pathways were not investigated in the previous theoretical studies on CH_2Cl.[13,19–21]

This article is organized as follows: in Sec. II, the theoretical methodology applied is described. In Sec. III, the results are presented and discussed. Finally, some conclusions are drawn in Sec. IV.

II. THEORETICAL METHODOLOGY

The electronic structure calculations on the CH_2Cl radical have been performed with the MOLPRO package[25] and the aug-cc-pVTZ basis set of Dunning.[26] Three dissociation pathways of CH_2Cl have been investigated and the corresponding PECs have been computed at the MRCI level[27] including the spin–orbit coupling for several electronic states. For each of the three pathways, in the calculation of the PECs, about 30 points were considered between 1 and 7 bohr along the corresponding reaction coordinates, namely, the C–Cl, C–H, and C–H_2 distances. For each of the different points along the reaction coordinate, the geometry in the remaining five coordinates of CH_2Cl was optimized (i.e., the equilibrium geometry of minimum energy in those coordinates was obtained) in the ground electronic state at the complete active space perturbation theory of second-order (CASPT2) level[28] with a minimal active space. These equilibrium geometries optimized in the ground state are also used in the calculation of the excited state curves. We used the same procedure previously applied for CH_2I[29] and CH_2Br.[30] The determination of the global minimum equilibrium geometry and harmonic frequencies was also carried out at this level. Once the geometries of the three reaction pathways were determined, the final PECs were computed at CASSCF and MRCI levels.[27,31] The spin–orbit coupling was introduced using the Breit–Pauli method implemented in MOLPRO[32] using the MRCI electronic wavefunction, and the eigenvalues of the full spin–orbit matrix that include the spin-free electronic states are computed to obtain the final spin–orbit states of the system.

As its homologues CH_2I and CH_2Br, CH_2Cl is a planar molecule and its genuine symmetry group is C_{2v}. To take advantage of the symmetry in order to reduce the computational cost, both Cl and H_2 elimination channels have been studied keeping this symmetry point group. In the case of the H elimination channel, the C_{2v} symmetry is broken, so the corresponding calculations were performed within the C_s symmetry group. Due to the presence of several Rydberg states[20] strongly affecting the Franck–Condon (FC) region in this system, it was found impossible to properly converge the calculations of this latter channel with an active space equivalent to that employed for the C_{2v} pathways, so a different active space had to be used.

For the elimination of chlorine and H_2, the following active space has been considered. At CASSCF level, the step where the orbitals are optimized, an active space of nine electrons in seven orbitals (7–9a_1, 2–3b_1, and 2–3b_2) was employed in a state-averaged CASSCF calculation including 13 doublet states (5A_1, 4B_1, 2B_2, and 2A_2) and six quartet states (2A_1, 2B_1, and 2A_2). To obtain more correlation and better describe some of the Rydberg states captured by our calculation, the active space was then slightly augmented in the MRCI calculations by adding one a_1 and one b_2 orbital (see the orbitals in the Appendix).

For the elimination of atomic hydrogen, it was found necessary to increase considerably the active space up to 13 electrons in 12 orbitals (6–14a' and 2–4a'') in order to describe reasonably the dissociation curves at the state-averaged CASSCF level. In addition, the number of states included in the state-averaged calculation was also reduced to 7 doublets (5A' and 2A'') and three quartets (2A' and 1A''). In this case, the same active space was employed at the MRCI level, but 5 $^2A''$ states were computed instead of 2 (these three additional states were not calculated in the state-averaged CASSCF calculation, as it was found impossible to keep the orbitals stable enough along the reaction coordinate if they were included). As a result, the curves associated with the H elimination channel are somewhat less accurate than those of the other two channels, but are still robust enough to describe the hydrogen atom elimination.

III. RESULTS AND DISCUSSION

A. Geometrical and energetic properties

Figure 1 shows the global minimum equilibrium geometry optimized in the ground electronic state for CH_2Cl showing the equilibrium distances and angles. These distances and angles are also presented in Table I, where they are compared to the values calculated in previous theoretical studies for CH_2Cl and with experimental values. Very good agreement is found between the present and the previously computed geometries, as well as with the experimental values. Our calculations indicate that the equilibrium structure of CH_2Cl is planar, as also found in earlier calculations.[21]

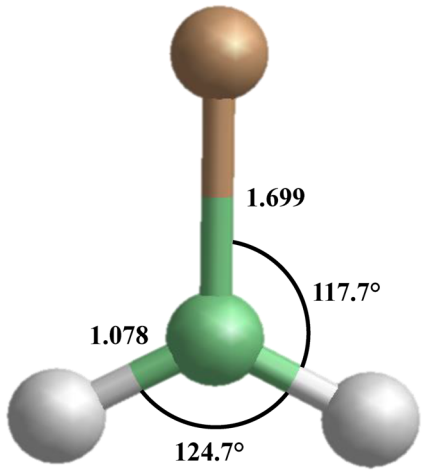

FIG. 1. Distances (in Å) and angles (in degree) associated with the equilibrium geometry optimized in the ground electronic state for CH_2Cl.

TABLE I. Equilibrium geometries and harmonic frequencies (calculated at the CASPT2 level) of the ground electronic state of CH_2Cl and Cl spin–orbit splitting (calculated at the MRCI + SO level) computed in this work, compared to previous theoretical and experimental data.

$CH_2Cl(C_{2v})$ 1^2B_1	(This work)	Theory[a]	Theory[b]	Theory[c]	Theory[d]	Exp.
$r_{C\text{-}H}$ (Å)	1.078	1.076	1.076	1.076	1.077	1.09[e]
$r_{C\text{-}Cl}$ (Å)	1.699	1.696	1.691	1.698	1.715	1.691[e]
$\widehat{HCH}$ (°)	124.7	124.4	124.2	124.4	125.1	122.6[e]
$\widehat{HCCl}$ (°)	117.65	117.8	117.9	117.8	117.45	118.7[e]
$\widehat{CClHH}$ (°)	180.0		180.0	180.0		
ν_1 (cm^{-1}) CH_2 s-stretch (a_1)	3155		3179	3169		
ν_2 (cm^{-1}) CH_2 scissors (a_1)	1410		1434	1415		1305[f], 1391[g]
ν_3 (cm^{-1}) CCl stretch (a_1)	843		868	835		827[f,g]
ν_4 (cm^{-1}) CH_2Cl umbrella (b_1)	189		168	229		402[f], 397[g]
ν_5 (cm^{-1}) CH_2 a-stretch (b_2)	3320		3335	3320		
ν_6 (cm^{-1}) CH_2 rock (b_2)	997		1004	997		1027[f]
Cl spin-orbit splitting (cm^{-1})	726					882[h]

[a]Reference 19, coupled-cluster (CCSD(T)) calculations using a 6-311 + +G(3df,3pd) basis.
[b]Reference 21, coupled-cluster (CCSD(T)) calculations using a 6-311 + +G(3df,3pd) basis.
[c]Reference 21, DFT/B3LYP calculations using a 6-311 + +G(3df,3pd) basis.
[d]Reference 22, DFT/B3LYP calculations using a 6-311G(d,p) basis.
[e]Reference 33.
[f]Reference 34.
[g]Reference 35.
[h]Reference 36.

TABLE II. Computed vertical excitation energies (in eV) with respect to the minimum of the ground state 1^2B_1, and squared dipole moments (in a.u.) for transitions to the first excited states of CH_2Cl, calculated at the MRCI level including spin–orbit coupling. The present energies and dipole moments are compared to previous *ab initio* MRCI and EOM-CCSD results, both of them not considering spin–orbit coupling, and to available experimental data. For those states with very close vertical excitation energies, the energy values are given with four decimal digits instead of with two. The symbols ∥ and ⊥ in parentheses to the right of the dipole moment values indicate the parallel or perpendicular character of the transition, respectively.

State	E_{ex}, this work	E_{ex}, theory[a]	E_{ex}, theory[b]	E_{ex}, exp.	μ^2, this work	μ^2, theory[b]
1	...	...	...	...	...	...
2	4.94	5.23	4.92	4.96–5.02[c]	0.0198 (⊥)	0.0423 (⊥)
3	5.3571	5.35	5.24		0.0025 (⊥)	...
4	5.3606	6.93	5.54		0.0069 (⊥)	0.0056 (⊥)
5	6.46	6.51	6.33	6.20[d]	0.3122 (∥)	0.4584 (∥)
6	6.53		6.34		...	...
7	6.92		6.72		0.0357 (⊥)	0.0505 (⊥)
8	7.52		8.02			...

[a]Reference 19, MRCI calculations using a cc-pVTZ basis.
[b]Reference 20, EOM-CCSD calculations using a 6-311 + +G(3df, 3pd) basis.
[c]References 12 and 37.
[d]Reference 9.

Harmonic frequencies of the six vibrational modes of CH_2Cl were also calculated and are collected and compared to previous theoretical and experimental frequencies presented in Table I. The present frequencies are very similar in general to the earlier theoretical ones. The current theoretical frequencies are also in very good agreement with the experimental ones, with the exception of ν_4, which is very much underestimated by the present (and also previous) simulations. The chlorine spin–orbit splitting calculated here (see Table I) is somewhat smaller than the experimental value, but still close to it.

In Table II, vertical excitation energies from the minimum of the ground state $1\,^2B_1$, and squared dipole moments for transitions to the first excited states of CH_2Cl, calculated at the MRCI level including the spin–orbit coupling (MRCI + SO), are presented and compared to those calculated by Li and Francisco[19] and Levchenko and Krylov,[20] as well as with the available experimental results. The present energies agree very well with those previously calculated, with the exception of the VEE calculated by Li and Francisco for the third excited state (6.93 eV). There is also a good qualitative agreement between the current dipole moments and those obtained by Levchenko and Krylov.[20] While Levchenko and Krylov[20] found no transition dipole moment for the second excited state (dark state), our calculations indicate that this state has associated a small but nonzero dipole moment.

Regarding the experimental information available on the position of the excited states, from the analysis of the microwave spectrum of CH_2Cl,[37] it was inferred that the minimum of the first excited state should be around 5.01 eV. Later on, in CH_2Cl photodissociation experiments in the 312–214 nm region, Reisler and co-workers[12] found a broad maximum in the product yield at ~250 nm (4.96 eV), associated with a perpendicular transition, which could correspond to the maximum of a transition between the ground and the first excited state. The current VEE of 4.94 eV, similarly to the energy of 4.92 eV of Ref. 20, is in excellent agreement with the experimental finding. Another strong ultraviolet absorption maximum was measured at ~200 nm (6.20 eV), with the associated peak extending up to ~215 nm.[9] Similarly, Reisler and co-workers[12] also detected a parallel transition in the excitation region of 240–214 nm. As mentioned above, the second excited state has a weak absorption associated. The third excited state (with VEE of 5.3606 eV) is a 3*s* Rydberg state for which *ab initio* calculations[13,20] have shown that in the Franck–Condon (FC) region, the strength of the transition dipole moment coupling to the ground state is nonzero but small as well. Our results presented in Table II also agree with this finding. Thus, this absorption maximum of around 200 nm was predominantly associated with a parallel transition to the fourth excited state.[9,12] The present VEE value of 6.46 eV, as well as the values of 6.51 and 6.33 eV of Refs. 19 and 20, respectively, are consistent with this transition. It is noted that the experimental ionization energy of CH_2Cl is 8.8 eV.[38] The good agreement between the currently calculated magnitudes of Tables I and II and the available experimental data assesses the quality of the present *ab initio* simulations for the ground and excited electronic states of CH_2Cl.

B. Potential-energy curves of the fragmentation pathways

The adiabatic PECs of CH_2Cl along the C–Cl and C–H bond distance, and along the C–H_2 distance, are shown for the ground and several excited states in Figs. 2–4, respectively. The upper panel of Figs. 2–4 shows the MRCI PECs, including the spin–orbit coupling. The symmetry of these PECs is difficult to assign when the spin–orbit coupling is considered, due to the mixing of states. For this reason, in the lower panel of the figures we present, the MRCI PECs are obtained without including the spin–orbit coupling. In this case, the symmetry of the PECs can be assigned both in the FC and in the asymptotic region, providing a clue on the symmetry of some of

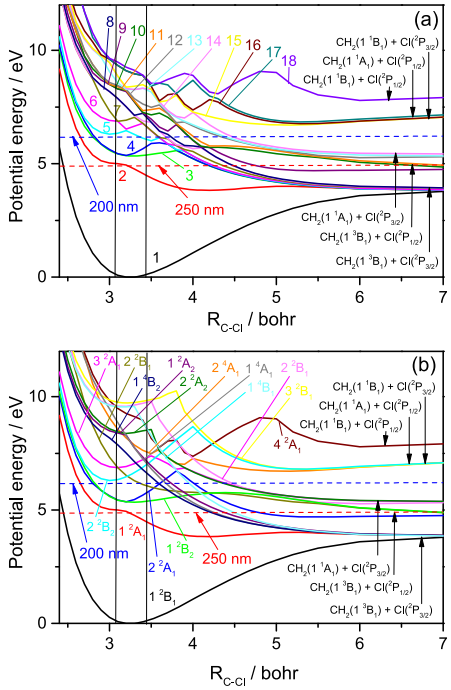

FIG. 2. Adiabatic potential-energy curves of the ground and excited electronic states of CH_2Cl along the C–Cl bond distance, calculated at the MRCI level (a) including and (b) not including the spin–orbit coupling. The two vertical lines denote the Franck–Condon region. The horizontal dashed lines mark the position of the maximum of the first absorption band at 250 nm (4.96 eV) and of the second absorption band at 200 nm (6.20 eV).

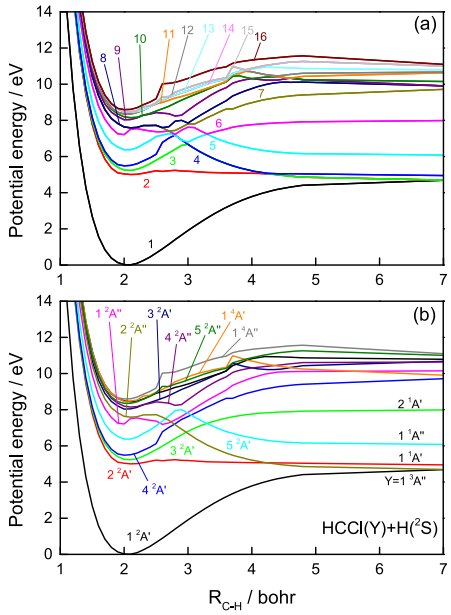

FIG. 3. Adiabatic potential-energy curves of the ground and excited electronic states of CH_2Cl along the C–H bond distance, calculated at the MRCI level (a) including and (b) not including the spin–orbit coupling.

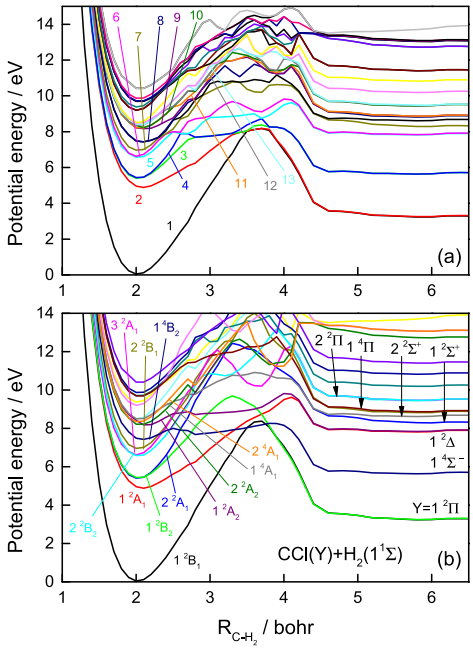

FIG. 4. Adiabatic potential-energy curves of the ground and excited electronic states along the C–H_2 distance (the distance between C and the center of mass of H_2), calculated at the MRCI level (a) including and (b) not including the spin–orbit coupling. Due to the lack of space in panel (b), it is not possible to include the labels of all the PECs, as shown in Fig. 2(b). However, they can be identified with the aid of Fig. 2(b) by means of the color code of the curves, which is the same as shown in Figs. 2(b) and 4(b).

the MRCI + SO PECs of the upper panel. The PECs with and without spin–orbit coupling are very similar in shape in the FC region and at short distances. Conversion of the crossings between uncoupled states in the spin-free representation into new avoided crossings when they become spin–orbit coupled reshapes the spin–orbit PECs. In the following, the possible dissociation mechanisms of these three fragmentation pathways will be analyzed and discussed in the light of the shape of the corresponding PECs.

1. Pathway CH_2 + Cl

In Fig. 2, the PEC of the first excited state exhibits a shallow well. However, in the FC region, what is accessed is the repulsive part of the PEC, which at 250 nm is well above the asymptote of the curve. Thus, a fast, direct dissociation of CH_2Cl into CH_2 + Cl is expected in this electronic state, producing an unstructured spectrum associated with the first absorption band.

The second and third excited states are very close in energy in the FC region. As mentioned above, these two states are optically very weakly coupled to the ground state. However, they could be populated by internal conversion from higher electronic states. It is interesting to note how the inclusion of the SO coupling significantly changes the shape of the excited state PECs from the MRCI picture of Fig. 2(b) to the MRCI + SO one of Fig. 2(a), due to the avoided crossings between states induced by the coupling. For instance, the

PEC of the third excited state (of $^2A_1$ symmetry) at MRCI level displays a relatively deep well and an avoided crossing at ~3.75 bohr, with a top exit barrier at about 6.7 eV. However, at the MRCI + SO level, an avoided crossing occurring between this third excited state and the fourth one (of $^2B_1$ symmetry) at ~3.5 bohr reduces remarkably (by more than 1 eV) the depth of the well and the height of the exit barrier of this state. A similar situation takes place for the second excited state at the MRCI level. An avoided crossing occurring at the MRCI + SO level between this state and the seventh excited state (of $^4B_2$ symmetry) at ~3.75 bohr also significantly lowers the well depth and barrier height of the second excited state. As a result, the PECs of these two states display shallower wells, followed by lower exit barriers at the MRCI + SO level than at MRCI one, and the second excited state becomes essentially a repulsive state in practice. It is noted that the two excited states with $^2A_1$ symmetry (the first and third excited states) of Fig. 2(b) exhibit a very similar shape to those calculated in Ref. 13 (see Fig. 2 of that work). The large effect of the SO coupling on the shape of the PECs indicates the importance of including this coupling even for atoms like Cl, where the coupling is not very large. In this sense, there are several evidences that intersystem crossing may be relevant in photodissociation and reaction dynamics of species bearing atoms of the periodic table third row.[39–41]

The MRCI + SO PECs of Fig. 2(a) show that the fourth and fifth excited states display an avoided crossing in the FC region. Further avoided crossings of these two states with lower and higher excited states at larger C–Cl distances outside the FC region, give their PECs the shape of essentially repulsive states, with very shallow wells and very low exit barriers. Again, for these two states, the effect of the SO coupling is very important in reshaping theirs PECs due to the numerous avoided crossings induced by the coupling. Such a reshaping of the PECs largely affects the fragmentation mechanisms in the different excited states. In the case of the fourth state, in the FC region, the repulsive part of the PEC located after the low exit barrier is populated at ~200 nm, leading to direct fragmentation of the radical producing a broad unstructured absorption spectrum, as found experimentally.[9] The fifth excited state is optically dark, and the PEC of the sixth excited state again exhibits a shallow well, a very low exit barrier, and the shape of a rather repulsive state, as a consequence of an avoided crossing produced by the SO coupling. Thus, a direct dissociation mechanism is expected in this case.

In the CH_2Cl photolysis experiments of Reisler and coworkers,[12] it was found that in the wavelength range 312–247 nm, the main products are $CH_2(1^3B_1)$ + $Cl(^2P_{3/2})$. Our PECs shown in Fig. 2 are consistent with this experimental result since all the PEC asymptotes below the energy of 250 nm correlate only with the $CH_2(1^3B_1)$ + $Cl(^2P_{3/2})$ products. In the range 240–214 nm (5.17–5.79 eV), both $Cl(^2P_{3/2})$ and $Cl(^2P_{1/2})$ fragments were found, with $CH_2(1^1A_1)$ as the main cofragment. Again, the PECs shown in Fig. 2 agree with this finding since in this range of energy, the asymptotes of the PECs correlate with the products $CH_2(1^3B_1)$ + $Cl(^2P_{1/2})$ and $CH_2(1^1A_1)$ + $Cl(^2P_{3/2})$.

For excitation wavelengths smaller than ~200 nm, the density of electronic states increases remarkably. The implication of this high density of states is that several of the electronic states with oscillator strength can be excited simultaneously at a given energy. Some of the PECs show one or more relatively high exit barriers, produced by avoided crossings between the PECs. All these states appear to be strongly coupled between them by nonadiabatic and spin–orbit couplings connecting the different excited PECs. Therefore, for excitation at energies higher than 7.0 eV, dissociation of CH_2Cl on various PECs is expected to occur, producing CH_2 and Cl fragments in a variety of electronic states and with a rather broad distribution of translational energies. The presence of relatively high barriers at distances larger than the FC region is likely to produce a rather slow dissociation mechanism. The exit barriers support tunneling resonances with an associated lifetime that will depend on the resonance position with respect to the top of the barrier.[42,43] In this situation, internal conversion to lower electronic states is predicted to take place, followed by predissociation combined with tunneling through the barriers.

2. Pathway HCCl + H

To the best of our knowledge, the fragmentation pathway into HCCl + H products has not been investigated experimentally. Thus, it is interesting to explore theoretically whether this pathway is possible, and if so, at what excitation wavelengths. The ground and excited state PECs at MRCI and MRCI + SO levels are shown in Fig. 3.

All the excited state PECs shown in Fig. 3 are bound with more or less deep wells. Same as shown in Fig. 2, the difference between the MRCI and the MRCI + SO PECs is that in the latter ones, more avoided crossing between curves are produced, causing the appearance of additional exit barriers. If we focus now on the MRCI + SO PECs shown in Fig. 3, it is noted that the first excited state PEC displays a very shallow well, and the shape of the curve is essentially that of a repulsive state. This situation is very similar to that previously found for the first excited state of the CH_2Br radical in the case of the dissociation pathway into HCBr and H fragments.[30] Since the asymptote of this state is slightly below 5 eV, the interesting implication is that for excitations at wavelengths <250 nm, a fast, direct dissociation into HCCl and H fragments should be possible. Thus, upon excitation of this electronic state, the present pathway would compete with that producing CH_2 + Cl.

The second and higher excited states exhibit relatively deep wells, with barriers and/or asymptotes high enough as to make dissociation rather unlikely in general. In the case of the third and fourth excited states (which carry a small but nonzero and a high oscillator strength,[20] respectively), excitation energies >7.2 eV would be required to overcome their exit barriers and produce dissociation. Higher states display very high-energy asymptotes. The PECs of Fig. 3(a) show that the wells of the excited states are, in general, partially embedded below the asymptote of the immediately lower electronic state. This situation favors that upon excitation of a given excited state, relaxation through internal conversion to rovibrationally excited states of the lower electronic states may occur. Once the first excited state is reached through internal conversion from higher states, dissociation would be possible. Combined with internal conversion, predissociation between different electronic states is another possible dissociation mechanism due to the nonadiabatic couplings associated with the several avoided crossings found in the PECs, also combined with tunneling through the exit barriers. Fluorescence to the ground state is a nondissociating mechanism to reach the lowest state from those excited states radiatively coupled to it.

It is noted, however, that all the above-mentioned dynamical mechanisms leading to dissociation (internal conversion, predissociation, and tunneling) are slow ones. Thus, the most likely possibility is that upon excitation to the second or higher excited states, the radical evolves to a much faster direct dissociation through pathway (4) to produce CH_2 + Cl. As discussed above, only a direct optical excitation of the first excited state would be effective to make possible dissociation through pathway (5).

3. Pathway CCl + H_2

Similarly to the PECs shown in Fig. 3, the excited state PECs along the C–H_2 dissociation distance shown in Fig. 4, are all bound, both at MRCI and MRCI + SO levels. The MRCI PECs display one or more exit barriers, while the MRCI + SO curves exhibit several additional barriers due to the conversion of many curve crossings into avoided ones upon inclusion of the SO coupling. The PECs of Fig. 4 differ from those of Fig. 3 in that their wells are much deeper, and they also show higher and more numerous exit barriers. In particular, the ground state exhibits a very high barrier. The deep well of the first excited state PEC shown in Fig. 4 is in sharp contrast with the essentially repulsive shape of the corresponding PEC shown in Fig. 3. Thus, in this situation of deep wells and high barriers shown by the several low-lying excited states, fast dissociation dynamics mechanisms are very likely to be prevented through this pathway at the excitation energies investigated experimentally so far, and even at higher energies.

As in the PECs shown in Fig. 3, the wells of practically all the excited states are, in general, partially embedded below the asymptote or the top of the barrier of the immediately lower electronic state (or states). Then, relaxation by internal conversion to lower electronic states is a possible mechanism. The difference with pathway (5) is that now the wells of several low-lying excited states are also embedded in the well of the ground state, and therefore, the internal conversion can populate highly excited rovibrational states of this electronic state. However, those rovibrational states would be located below the top of the exit barrier, and dissociation would require the occurrence of a slow tunneling process. A faster and more likely mechanism is that these rovibrational states populated in the ground electronic state by internal conversion dissociate through pathways (4) and (5), for which there is no exit barrier in the ground state. The same holds once the first excited state is also populated by internal conversion. In this case, dissociation will also occur through pathways (4) and (5), for which the PEC of this state is essentially repulsive. Predissociation and tunneling through the exit barriers are possible mechanisms in addition to internal conversion, for excitation to the different excited states. However, such mechanisms are very slow as well, and they will not compete with the fast direct dissociation occurring in the essentially repulsive PECs of the corresponding excited states through pathway (4). The implication is that the much longer time scales involved in pathway (6) make it very unlikely to occur.

It is noted that there is a strong similarity between the shape of the PECs of Figs. 2–4 and the corresponding PECs previously calculated for the same dissociation pathways of the CH_2Br radical.[30] Potential-energy curves with a similar shape to those of CH_2Br and CH_2Cl are also found for the $CH_2I \rightarrow CH_2 + I$ fragmentation pathway [the PECs associated with the pathways equivalent to the (5) and (6) ones were not calculated for CH_2I].[29] This result indicates that a qualitatively similar photodissociation dynamics behavior should be expected from the CH_2X radicals with X = Cl, Br, and I.

The potential curves shown in Figs. 2–4 and the previous discussion of the possible associated dynamical mechanisms indicate that the CH_2Cl radical can undergo a fast dissociation in essentially repulsive excited states through pathways (4) and (5), while this fragmentation appears very unlikely through pathway (6). In the case of pathway (4), Fig. 2 shows that absorption of the first excited state in the Franck–Condon region begins at around 4.67 eV (265 nm). At higher energies, other excited states such as the fourth and the sixth ones (in addition to the first one) absorb as well, in agreement with the experimental findings.[9,12,13,37] The curves of Fig. 3 indicate that fast fragmentation through pathway (5) into HCCl + H, although not yet observed experimentally, is also possible upon excitation only to the first excited state. In order to overcome the very low exit barrier of the PEC of this state (see Fig. 3), excitation leading to dissociation should begin at energies slightly higher than 5 eV (<250 nm). Excitation to higher excited states would not cause fast enough dissociation mechanisms through this pathway as to compete with those of pathway (4), same as it happens with pathway (6) for excitation to any excited electronic state. It is noted that the HCCl radical formed through pathway (5) could undergo further photodissociation into CH + Cl, then becoming an additional source of Cl atoms in the atmosphere.

To analyze the atmospheric implications of the CH_2Cl photodissociation, we must consider the magnitude of the actinic fluxes of solar irradiation at the required wavelengths at the different atmospheric (tropospheric and stratospheric) altitudes. Significantly high solar actinic fluxes are found for the wavelength range 285–370 nm (3.35–4.35 eV) at altitudes from above sea level (lower troposphere) up to 30 km (middle–upper stratosphere, where ozone abundance reaches a maximum[2]). However, in this range of wavelengths, absorption of CH_2Cl in the first excited state is either very weak or inexistent. Actinic fluxes available in the 190–230 nm (5.39–6.53 eV) range at stratospheric altitudes are two orders of magnitude weaker, but still appreciable. Since a maximum in the absorption of CH_2Cl has been found at 200 nm, with the associated peak covering the range 198.5–215 nm,[9] it is expected that CH_2Cl will absorb appreciably in atmospheric regions, where ozone is abundant. In the 190–230 nm wavelength range, the pathways (4) and (5) are possible, as discussed above. Thus, in addition to the Cl atoms generated by pathway (4), HCCl radicals can be also produced which could further photodissociate in the atmosphere, contributing to ozone depletion as well.

IV. CONCLUSIONS

Photodissociation of the CH_2Cl radical is investigated by means of high-level multireference configuration interaction *ab initio* calculations, including the spin–orbit coupling. All possible fragmentation pathways of the radical, namely, $CH_2Cl + h\nu \rightarrow CH_2 + Cl$, HCCl + H, and CCl + H_2 are analyzed. Potential-energy curves associated with the ground and several excited electronic states along the dissociating bond distance corresponding to each pathway are obtained. To the best of our knowledge, this is the first time that all the photodissociation pathways of this radical are studied and that spin–orbit effects are considered. An interesting finding is that including the spin–orbit coupling dramatically changes the shape of

most of the calculated potential-energy curves due to the conversion of several crossings between curves into avoided crossings when the coupling is added. The appearance of these additional avoided crossings produces shallower wells and additional (generally low) exit barriers in the potential curves that determine completely their final shape and, therefore, the possible photodissociation dynamics mechanisms that can take place in the different excited states. Thus, including the spin–orbit coupling is crucial to understand the photodissociation dynamics of this radical.

Analysis of the shape of the calculated potential-energy curves allows one to elucidate the possible photofragmentation dynamical mechanisms. Dissociation of CH_2Cl into CH_2 + Cl proceeds through a fast direct dissociation mechanism in the low-lying excited states, which are essentially repulsive. The position of the calculated potential curves is consistent with the available experimental findings regarding absorption spectra and product fragments detected. The same mechanism holds for dissociation into HCCl + H in the first excited state. For higher excited states of this latter pathway, as well as for all the excited states of the pathway leading to CCl + H_2, the appearance of avoided crossings between states and high exit barriers leads to remarkably slower dissociation mechanisms. Thus, the pathways producing CH_2 + Cl and HCCl + H (in the first excited state) by means of faster mechanisms are expected to be the dominant ones, while the much slower pathway producing CCl + H_2 is predicted to be unlikely. While the experimental studies have focused so far on the pathway leading to CH_2 + Cl, the present results indicate that searching experimentally for the fragmentation pathway producing HCCl + H should also be interesting. The shape of the CH_2Cl potential curves is found to be qualitatively similar to those previously obtained for CH_2Br and CH_2I, so the three radicals are expected to also exhibit a similar photodissociation dynamics behavior.

Regarding the atmospheric impact of CH_2Cl photodissociation, solar irradiation actinic fluxes available in the 190–230 nm (5.39–6.53 eV) range at stratospheric altitudes, where ozone is abundant, are significant. It has been found experimentally that in this wavelength range, some of the low-lying excited states of CH_2Cl can absorb (a CH_2Cl absorption maximum was observed at 200 nm). The present results show that in this excitation energy range, the pathways leading to CH_2 + Cl and to HCCl + H products are open, and the HCCl radicals formed could further photodissociate into CH + Cl in the atmosphere, also contributing to the Cl atom budget. Thus, these two dissociation pathways could contribute to ozone depletion.

ACKNOWLEDGMENTS

This research was carried out within the Unidad Asociada Química Física Molecular between the Departamento de Química Física of Universidad Complutense de Madrid and CSIC. This work was funded by the Ministerio de Ciencia e Innovación (MCIN, Spain) under Grant Nos. PID2021-122549NB-C21, PID2021-122796NB-I00, and PID2021-122839NB-I00. This project received funding from the European Union's Horizon 2020 research and innovation programme under Marie Skłodowska-Curie Grant Agreement No. 872081 and from the European Research Council

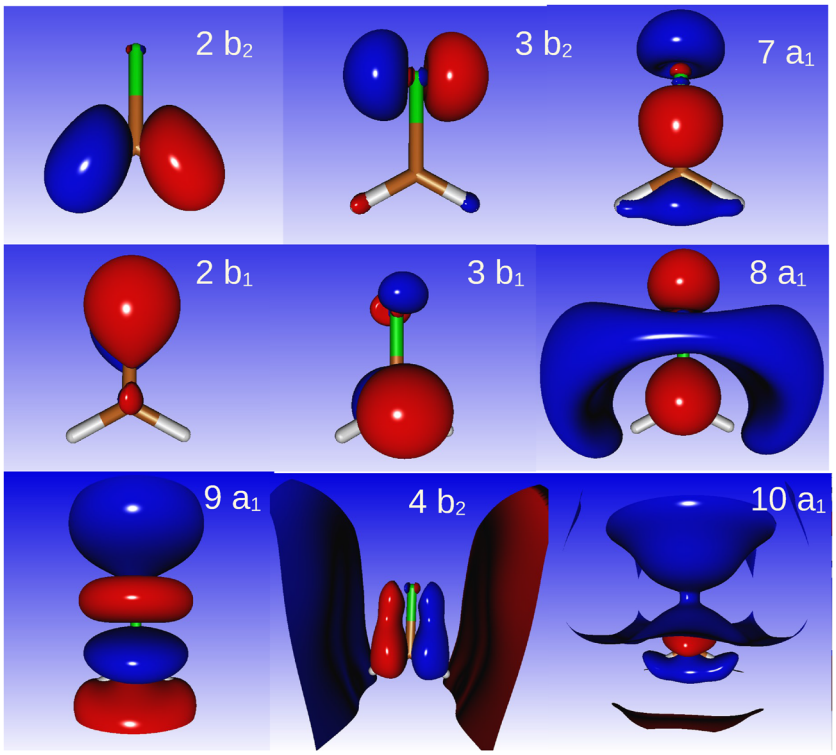

FIG. 5. Representation of the state-averaged CASSCF orbitals included in the active space of pathways (4) and (6). It is noted that the full spatial extension of the Rydberg orbitals ($4b_2$ and $10a_1$) cannot be captured in the figure due to their diffuse character.

COST Action CA21101 (COSY). The authors acknowledge the Centro de Supercomputación de Galicia (CESGA, Spain) for the use of its resources.

AUTHOR DECLARATIONS

Conflict of Interest

The authors have no conflicts to disclose.

Author Contributions

F. Charfeddine: Data curation (equal); Formal analysis (equal); Investigation (equal); Visualization (equal). **O. Yazidi**: Conceptualization (equal); Data curation (equal); Formal analysis (equal); Investigation (equal); Visualization (equal); Writing – review & editing (equal). **A. Zanchet**: Conceptualization (lead); Supervision (lead); Validation (lead); Writing – review & editing (equal). **L. Bañares**: Conceptualization (equal); Funding acquisition (lead); Supervision (lead); Validation (lead); Writing – review & editing (equal). **A. García-Vela**: Conceptualization (equal); Funding acquisition (lead); Supervision (lead); Validation (equal); Writing – original draft (lead); Writing – review & editing (equal).

DATA AVAILABILITY

The data that support the findings of this study are available within the article.

APPENDIX: STATE-AVERAGED CASSCF ORBITALS

In Fig. 5, the state-averaged CASSCF orbitals included in the active space of dissociation pathways (4) and (6) are shown.

REFERENCES

[1]R. A. Moss, M. Platz, M. Jones *et al.*, *Reactive Intermediate Chemistry* (Wiley Online Library, 2004).
[2]B. J. Finlayson-Pitts and J. N. Pitts, *Chemistry of the Upper and Lower Atmosphere: Theory, Experiments, and Applications* (Academic, New York, 1999).
[3]J. S. Francisco and M. M. Maricq, "Atmospheric photochemistry of alternative halocarbons," in *Advances in Photochemistry* (Wiley, New York, 1995), Vol. 20, pp. 79–163.
[4]W. R. Simpson, S. S. Brown, A. Saiz-Lopez, J. A. Thornton, and R. von Glasow, "Tropospheric halogen chemistry: Sources, cycling, and impacts," Chem. Rev. **115**, 4035–4062 (2015).
[5]M. A. Navarro, E. L. Atlas, A. Saiz-Lopez, X. Rodriguez-Lloveras *et al.*, "Airborne measurements of organic bromine compounds in the Pacific tropical tropopause layer," Proc. Natl. Acad. Sci. U. S. A. **112**(45), 13789–13793 (2015).
[6]A. Saiz-Lopez, R. P. Fernandez, Q. Li *et al.*, "Natural short-lived halogens exert an indirect cooling effect on climate," Nature **618**, 967–973 (2023).
[7]E. Tschuikow-Roux, T. Yano, and J. Niedzielski, "Reactions of ground state chlorine atoms with fluorinated methanes and ethanes," J. Chem. Phys. **82**(1), 65–74 (1985).
[8]T. J. Wallington, J. M. Andino, J. C. Ball, and S. M. Japar, "Fourier transform infrared studies of the reaction of Cl Atoms with PAN, PPN, CH_3OOH, HCOOH, CH_3COCH_3 and $CH_3COC_2H_5$ at 295 ± 2 K," J. Atmos. Chem. **10**(3), 301–313 (1990).
[9]P. B. Roussel, P. D. Lightfoot, F. Caralp, V. Catoire, R. Lesclaux, and W. Forst, "Ultraviolet absorption spectra of the CH_2CI and $CHCl_2$ radicals and the kinetics of their self-recombination reactions from 273 to 686 K," J. Chem. Soc., Faraday Trans. **87**(15), 2367–2377 (1991).
[10]J. A. Seetula and I. R. Slagle, "Kinetics of the reaction of the CH_2Cl radical with oxygen atoms," Chem. Phys. Lett. **277**, 381–386 (1997).
[11]J. A. Seetula, "Kinetics of the R + Cl_2 (R = CH_2Cl, $CHBrCl$, CCl_3 and CH_3CCl_2) reactions. An *ab initio* study of the transition states," J. Chem. Soc., Faraday Trans. **94**(24), 3561–3567 (1998).
[12]V. Dribinski, A. B. Potter, A. V. Demyanenko, and H. Reisler, "Photodissociation dynamics of the CH_2Cl radical: Ion imaging studies of the Cl+CH_2 channel," J. Chem. Phys. **115**(16), 7474–7484 (2001).
[13]S. V. Levchenko, A. V. Demyanenko, V. L. Dribinski, A. B. Potter, H. Reisler, and A. I. Krylov, "Rydberg–valence interactions in $CH_2Cl \rightarrow CH_2$ + Cl photodissociation: Dependence of absorption probability on ground state vibrational excitation," J. Chem. Phys. **118**(20), 9233–9240 (2003).
[14]H.-T. Ma, C.-Y. Shi, W.-S. Bian, H.-M. Su, and F.-A. Kong, "Reaction of CH_2Cl with O_2," Chin. J. Chem. Phys. **20**(4), 383–387 (2007).
[15]M. Hold, K. Hoyermann, I. Morozov, and T. Zeuch, "CH_2Cl and $CHCl_2$ radical chemistry: The formation by the reactions CH_3Cl + F and CH_2Cl_2 + F and the destruction by the reactions CH_2Cl + O and $CHCl_2$ + O," Z. Phys. Chem. **223**, 409–426 (2009).
[16]Z. Yang, K. Schnorr, A. Bhattacherjee, P.-L. Lefebvre, M. Epshtein, T. Xue, J. F. Stanton, and S. R. Leone, "Electron-withdrawing effects in the photodissociation of CH_2ICl to Form CH_2Cl radical, simultaneously viewed through the carbon K and chlorine $L_{2,3}$ X-ray edges," J. Am. Chem. Soc. **140**(41), 13360–13366 (2018).
[17]J. A. Seetula, "Kinetics and thermochemistry of the R + HBr ⇔ RH + Br (R = CH_2Cl, $CHCl_2$, CH_3CHCl or CH_3CCl_2) equilibrium," J. Chem. Soc., Faraday Trans. **92**(17), 3069–3078 (1996).
[18]M. P. Rissanen, A. J. Eskola, and R. S. Timonen, "Kinetics of the reactions of CH_2Cl, CH_3CHCl, and CH_3CCl_2 radicals with Cl_2 in the temperature range 191-363 K," J. Phys. Chem. A **223**(14), 4805–4810 (2010).
[19]Y. Li and J. S. Francisco, "CASSCF and MRCI studies of the electronic excited states of CH_2Cl and CH_2Br," J. Chem. Phys. **114**(7), 2879–2882 (2001).
[20]S. V. Levchenko and A. I. Krylov, "Electronic structure of halogen-substituted methyl radicals:Excited states of CH_2Cl and CH_2F," J. Chem. Phys. **115**(16), 7485–7494 (2001).
[21]S. V. Levchenko and A. I. Krylov, "Electronic structure of halogen-substituted methyl radicals: Equilibrium geometries and vibrational spectra of CH_2Cl and CH_2F," J. Phys. Chem. A **106**(20), 5169–5176 (2002).
[22]J.-X. Zhang, Z.-S. Li, J.-Y. Liu, and C.-C. Sun, "Radical–molecule reaction CH_2Cl + NO_2: A mechanistic study," Theor. Chem. Acc. **117**, 579–586 (2007).
[23]T. J. Sears, F. Temps, H. G. Wagner, and M. Wolf, "Far-infrared laser magnetic resonance spectroscopy of CH_2Cl ($\tilde{X}\ ^2B_1$)," J. Mol. Spectrosc. **168**, 136–146 (1994).
[24]A. B. Potter, V. Dribinski, A. V. Demyanenko, and H. Reisler, "Competitive channels in the jet-cooled photodissociation of the CH_2Cl radical," Chem. Phys. Lett. **349**, 257–265 (2001).
[25]H.-J. Werner *et al.*, *MOLPRO, version 2015.1, a package of ab initio programs*, 2015, see http://www.molpro.net.
[26]T. H. Dunning, Jr., "Gaussian basis sets for use in correlated molecular calculations. I. The atoms boron through neon and hydrogen," J. Chem. Phys. **90**(2), 1007–1023 (1989).
[27]H.-J. Werner and P. J. Knowles, "An efficient internally contracted multiconfiguration-reference configuration interaction method," J. Chem. Phys. **89**, 5803–5814 (1988).
[28]H.-J. Werner, "Third-order multireference perturbation theory: The CASPT3 method," Mol. Phys. **89**, 645–661 (1996).
[29]A. Bouallagui, A. Zanchet, L. Bañares, and A. García-Vela, "An *ab initio* study of the photodissociation of CH_2I and CH_2I^+," Phys. Chem. Chem. Phys. **25**(30), 20365–20372 (2023).
[30]F. Charfeddine, A. Zanchet, O. Yazidi, C. A. Cuevas, A. Saiz-Lopez, L. Bañares, and A. García-Vela, "Photodissociation of the CH_2Br radical: A theoretical study," J. Chem. Phys. **160**(7), 074301 (2024).
[31]H.-J. Werner and P. J. Knowles, "A second order multiconfiguration SCF procedure with optimum convergence," J. Chem. Phys. **82**, 5053–5063 (1985).

[32]A. Berning, M. Schweizer, H.-J. Werner, P. J. Knowles, and P. Palmieri, "Spin-orbit matrix elements for internally contracted multireference configuration interaction wavefunctions," Mol. Phys. **98**(21), 1823–1833 (2000).
[33]D. R. Lide, *CRC Handbook of Chemistry and Physics* (CRC Press, Boca Raton, FL, 1999).
[34]M. E. Jacox and D. E. Milligan, "Matrix-isolation study of the vacuum-ultraviolet photolysis of methyl chloride and methylene chloride. Infrared and ultraviolet spectra of the free radicals CCl, H_2CCl, and CCl_2," J. Chem. Phys. **53**(7), 2688–2701 (1970).
[35]L. Andrews and D. W. Smith, "Matrix infrared spectrum and bonding in the monochloromethyl radical," J. Chem. Phys. **53**(7), 2956–2966 (1970).
[36]M. Dagenais, J. W. C. Johns, and A. R. W. McKellar, "Precise measurement of the ground state ($^2P_{1/2}$–$^2P_{3/2}$) splitting of atomic chlorine by CO_2 laser Zeeman spectroscopy," Can. J. Phys. **54**(14), 1438–1441 (1976).
[37]Y. Endo, S. Saito, and E. Hirota, "The microwave spectrum of the chloromethyl radical, CH_2Cl," Can. J. Phys. **62**(12), 1347 (1984).
[38]F. P. Lossing, "Free radicals by mass spectrometry XLIV. Ionization potentials and bond dissociation energies for chloro- and fluoro-methyl radicals," Bull. Soc. Chim. Belg. **81**(1), 125–134 (1972).
[39]A. Chichinin, T. S. Einfeld, K.-H. Gericke, J. Grunenberg, C. Maul, and L. V. Schäfer, "Photodissociation dynamics of $SOCl_2$," Phys. Chem. Chem. Phys. **7**, 301–309 (2005).
[40]S. Mai, M. Pollum, L. Martínez-Fernández, N. Dunn, P. Marquetand, I. Corral, C. E. Crespo-Hernández, and L. González, "The origin of efficient triplet state population in sulfur-substituted nucleobases," Nat. Commun. **7**, 13077 (2016).
[41]A. Zanchet, O. Roncero, E. Karabulut, N. Solem, C. Romanzin, R. Thissen, and C. Alcaraz, "The role of intersystem crossing in the reactive collision of $S^+(^4S)$ with H_2," J. Chem. Phys. **161**, 044302 (2024).
[42]A. García-Vela, R. B. Gerber, D. G. Imre, and J. J. Valentini, "Quantum resonances and interference effects in the UV photodissociation of Ar HCl," Chem. Phys. Lett. **202**(6), 473–478 (1993).
[43]A. García-Vela, "Highly delocalized orbiting resonances," J. Chem. Phys. **129**(9), 094307 (2008).